Geophysical Research Letters

RESEARCH LETTER
10.1029/2019GL086206

In Situ Observations of the Diurnal Variation in the Boundary Layer of Mature Hurricanes

Jun A. Zhang[1,2], **Jason P. Dunion**[1,2], **and David S. Nolan**[3]

[1]Hurricane Research Division, NOAA/AOML, Miami, FL, USA, [2]Cooperative Institute for Marine and Atmospheric Sciences, University of Miami, Miami, FL, USA, [3]Department of Atmospheric Sciences, University of Miami, Miami, FL, USA

Key Points:
- Dropsonde data from mature hurricanes are composited to study the diurnal variation of the boundary layer structure
- Both the inflow speed and moist entropy values are greater in the nighttime boundary layer than in the daytime boundary layer
- The diurnal cycle of tropical cyclone low-level structure is strongest at a radius range of 250–500 km

Supporting Information:
- Supporting Information S1

Correspondence to:
J. A. Zhang,
jun.zhang@noaa.gov

Citation:
Zhang, J. A., Dunion, J. P., & Nolan, D. S. (2020). In situ observations of the diurnal variation in the boundary layer of mature hurricanes. *Geophysical Research Letters*, *47*, 2019GL086206. https://doi.org/10.1029/2019GL086206

Received 12 NOV 2019
Accepted 14 JAN 2020
Accepted article online 16 JAN 2020

Abstract Recent studies have suggested that the structure of tropical cyclones (TCs), especially the upper-level clouds as indicated by satellite infrared brightness temperatures and precipitation, fluctuates with the diurnal cycle. The diurnal cycle of the low-level structure, including the boundary layer, has not yet been investigated with observations. This study analyzes data from 2242 GPS dropsondes collected in mature hurricanes to investigate the diurnal variation of the mean boundary layer structure. A composite analysis is conducted to compare the kinematic and thermodynamic structure during nighttime (0–6 local time) vs in the afternoon (12–18 local time). The composites show that much stronger inflow occurs during nighttime and the moist entropy is also larger than that in the daytime. Grouping the dropsonde data into 6-h time windows relative to the local time shows a clear diurnal signal of boundary layer inflow. The amplitude of the diurnal signal is largest at a radius of 250–500 km.

Plain Language Summary The upper-level clouds that we see in satellite images of tropical cyclones (also known as hurricanes) are often seen to expand and contract over the course of each day. These expansions are associated with a pulse of thunderstorms and rain that travel hundreds of kilometers away from the storm center. Although this daily cycle at upper levels of the atmosphere is well established, it remains unknown whether there are similar changes in winds and moisture near the surface. This study uses observations from hundreds of dropsondes – instruments on parachutes that are dropped out of airplanes – to determine whether there are similar daily changes in the hurricane winds at low altitudes. These winds are indeed shown to have a daily pattern, with stronger inflow (wind flowing toward the storm center) and increased moisture occurring in the overnight hours as compared to the rest of the day. These periods of increased inflow and moisture precede the outward moving bands of thunderstorms, and then diminish as the bands steadily move outward to larger distances. This study could help us better understand how the TC diurnal cycle affects the low-level structure of storms.

1. Introduction

The diurnal variation of precipitation and convection over the tropical oceans has been recognized for several decades (e.g., Browner et al., 1977; Gray & Jacobson, 1977; Randall et al., 1991; Liu & Moncrieff, 1998; Ruppert & Hohenegger, 2018; Yang & Slingo, 2001). Recent observational studies have suggested that the structure of tropical cyclones (TCs), especially the upper-level clouds as measured by satellite infrared brightness temperatures, tend to vary following a diurnal cycle and/or semi diurnal cycle (e.g., Bowman & Fowler, 2015; Ditchek, Corbosiero, et al., 2019; Ditchek, Molinari, et al., 2019; Dunion et al., 2014; Kossin, 2002; Knaff et al., 2019; Leppert & Cecil, 2016; Wu & Ruan, 2016). Analyses of a 10 year data set of storm-centered infrared satellite images suggested that the TC diurnal cycle may be tied to hurricane dynamics, structure and intensity change (Dunion et al., 2014).

Numerical studies have also confirmed the diurnal cycle of TC structure at both the genesis (Melhauser & Zhang, 2014) and mature stages (Ruppert & O'Neill, 2019; Tang & Zhang, 2016) with attention to how radiation affects the structure and diurnal cycle of TCs. O'Neill et al. (2017) investigated the possible mechanisms that are responsible for the diurnal pulsing of clouds near the TC outflow layer and found diurnal waves that have characteristics of internal gravity waves forced by heating in the TC inner core. Many previous studies have documented boundary layer structure change in response to the diurnal cycle in non-TC conditions

(e.g., Betts et al., 2002; Kumar et al., 2010; Mellor & Yamada, 1974; Svensson, 2011). In global models, the diurnal variation of boundary layer properties is very important (Holtslag et al., 2013), especially in the stable boundary layer over land. Over the ocean, Liu and Liang (2010) found that the boundary layer height varies with the diurnal cycle in non-TC conditions. Additionally, Dunion et al. (2019) examined a hurricane nature run (Nolan et al., 2013) and found strong diurnal variations of boundary layer inflow and surface winds. However, these variations have not yet been identified in observations.

The purpose of this paper is to use in situ observations to investigate how the TC boundary layer structure varies with the diurnal cycle in mature hurricanes. Both kinematic and thermodynamic structures are studied, including inflow strength, boundary layer depth, and moisture distribution.

2. Data and Analysis Method

GPS dropsonde data are analyzed to study the diurnal variation of the boundary layer structure using a composite analysis method. A detailed description of dropsonde specifications and performance can be found in Hock and Franklin (1999). Dropsondes from 295 hurricane research and reconnaissance flights (NOAA WP-3D, G-IV, and Air force C-130 s) in 20 hurricanes are postprocessed. A total of 2,242 dropsondes that have observations of wind, temperature, and humidity from flight level to ocean with no gaps (i.e., there are no missing data between the aircraft flight level and the surface) are used in the final analysis. The purpose here is to exclude dropsondes that terminate before they reach the maximum boundary layer inflow that is typically located at ~100 m altitude (Zhang et al., 2011). Following Dunion et al. (2014), we restrict to data collected in mature hurricanes ($V_{max} \geq 43$ m/s, where V_{max} is the maximum 1 min surface wind speed). Data distribution and information are shown in the Supporting Information S1. We composite the dropsonde data in a similar manner to Zhang et al. (2011, 2013). When compositing the data, the radial bin width is 20 km for the inner core ($R < 100$ km), and it is 50 km for the outer region of the storm. Data are grouped relative to the local time (LT) in four periods: night (0–6 LT), morning (6–12 LT), afternoon (12–18 LT), and evening (18–24 LT). Note that the derived variables are computed for each dropsonde before composite analysis.

3. Results

The differences in the composites between the night (0–6 LT) and afternoon (12–18 LT) groups are investigated first, as these time periods were found to have significant TC diurnal-cycle differences in previous satellite studies (e.g., Dunion et al., 2014). Radius-height (*R*-*Z*) plots of the azimuthally averaged tangential wind speed (Figures 1a and 1b) generally show similar structure between the night and afternoon composites. It is also evident that the maximum tangential wind speed is located at a height of ~700 m for both groups (Figures 1a and 1b). The maximum value of the tangential wind speed is statistically significantly larger in the night composite than in the afternoon composite following a *t* test, although the difference is relatively small (~5 m/s). Near the surface, the difference in the tangential wind speed is not statistically significant between the two composites (Figure 1c). The wind field is also found to be broader in the nighttime than in the afternoon, especially for radii >300 km. These findings generally agree with a recent study that examined diurnal variability of tangential wind in a realistic hurricane simulation (Dunion et al., 2019). The height of the maximum tangential wind speed (as indicated by the dashed black line) shows similar radial variation between the two groups, although it is slightly elevated during nighttime.

Radial wind speed shows a clear difference between the night and afternoon periods (Figures 1d–1f). It is evident that the nighttime composite has stronger inflow near the eyewall region than the afternoon composite (Figure 1f), and this difference is statistically significant at 95% confidence based on the *t* test. The peak inflow in the night composite is 17.7 m/s while it is only 15.3 m/s in the afternoon composite. There is a "moat" region (i.e., $R = 150$–200 km from storm center) where the difference in the radial wind speed is relatively small between the two composites. At larger radii ($R > 200$ km), there is statistically significant difference in the radial wind speed between the two composites, with the inflow layer at night being stronger than in the afternoon out to a radius of ~500 km (Figure 1f). This finding is consistent with Dunion et al. (2019). The TC inflow layer is also deeper at night than in the afternoon at outer radii (i.e., $R = 200$–500 km), as indicated by the black line which denotes the top of the inflow layer defined as the height of 10% maximum inflow following Zhang et al. (2011).

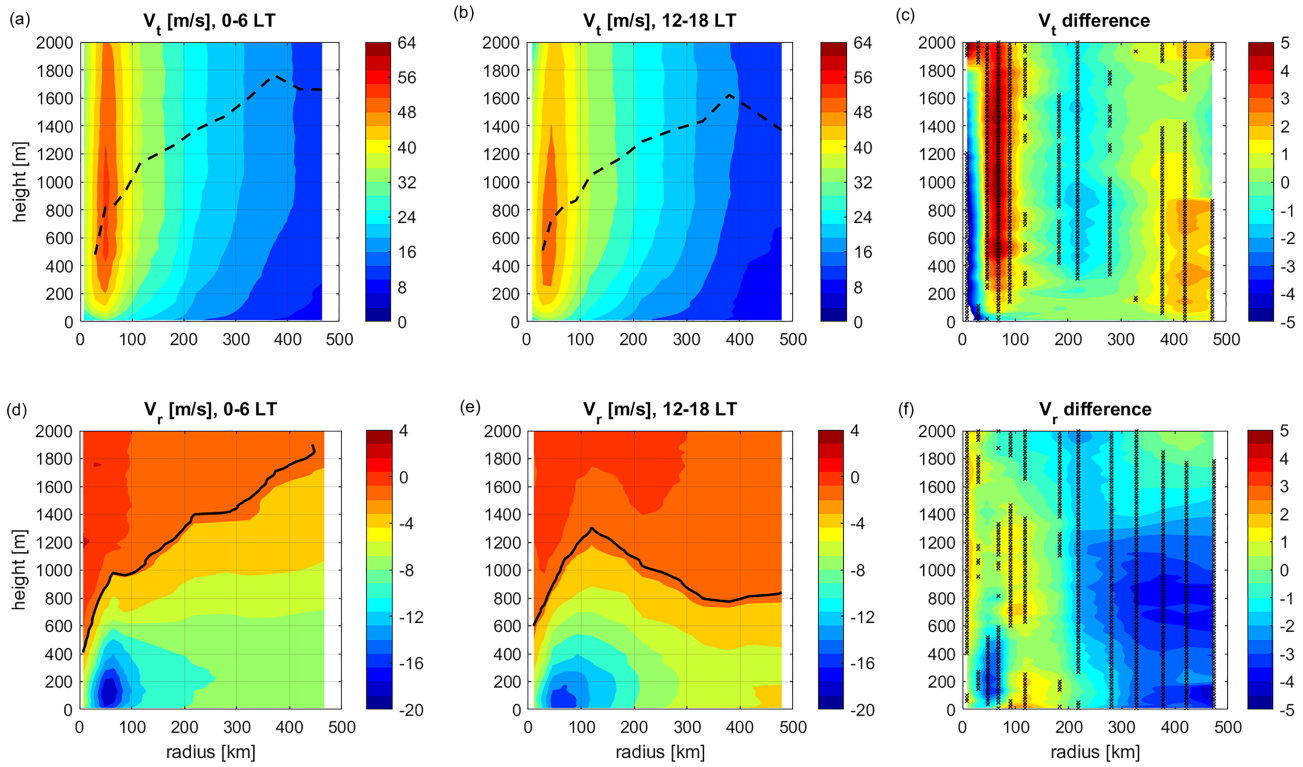

Figure 1. Dropsonde composites of tangential wind (V_t, upper panels) and radial wind (V_r, lower panels) for nighttime (0–6 LT, left panels) and afternoon (12–18 LT, middle panels). The difference fields are shown in the right panels. The black dashed line shows the height of the maximum V_t and the black solid line shows the inflow layer depth. The vertical stipples show regions where the difference is statistically significant at the 95% confidence level following a *t* test.

Composites of thermodynamic fields also show substantial differences between night and afternoon. Radius-height plots of relative humidity are shown in Figure 2a (night) and Figure 2b (afternoon). It is evident that the relative humidity is statistically significantly larger at night than in the afternoon at all locations except the moat region (Figure 2c). In the inner-core region (i.e., $R < 100$ km), the relative humidity is as high as 95% in the night, while it only reaches 90% in the afternoon. The contour of 90% relative humidity (black line) extends to ~2 km altitude in the night composite, while it only extends to ~1.3 km altitude in the afternoon composite. Near the top of the TC inflow layer, the 85% contour (black dashed line) extends outward to a radius of ~475 km at night, while it only extends out to ~250 km in the afternoon. These tendencies for the radial extent of low-level moisture to be enhanced (suppressed) in the night (afternoon) were also found by Dunion et al. (2019) in the numerical simulation. The equivalent potential temperature (θ_e) is compared between the night and afternoon composites in Figures 2d and 2e, showing a similar structure in the eyewall region with the constant θ_e contour being nearly vertical in the eyewall (R ~ 50 km). Note that we compute θ_e following Bolton (1980) in the form of: $\theta_e = \theta exp\left(\frac{L_v q}{c_p T_{LCL}}\right)$, where T_{LCL} represents the lifting condensation level temperature, c_p is the specific heat of air (at constant pressure), L_v is latent heat of vaporization, q is specific humidity, and θ is the potential temperature. The magnitude of θ_e close to the storm center ($R \leq 50$ km) is statistically significantly larger in the night composite than in the afternoon composite (Figure 2f). At outer radii, the largest difference in θ_e is seen at radii of 250–350 km, where θ_e is also statistically significantly larger in the nighttime than in the afternoon. Overall, the boundary layer θ_e is larger in the night than in the afternoon at all vertical levels at $R > 150$ km. The enhancement of θ_e at night may be related to the development of deep convection which propagates outward during the daytime as shown by Dunion et al. (2019). It is also possible that the deeper and stronger inflow at night favors the development of convection through enhanced boundary layer convergence and/or turbulent mixing. It is shown in Figure 2i that the thermodynamic mixed layer is more unstable at $R > 200$ km at night than in the afternoon. However, the

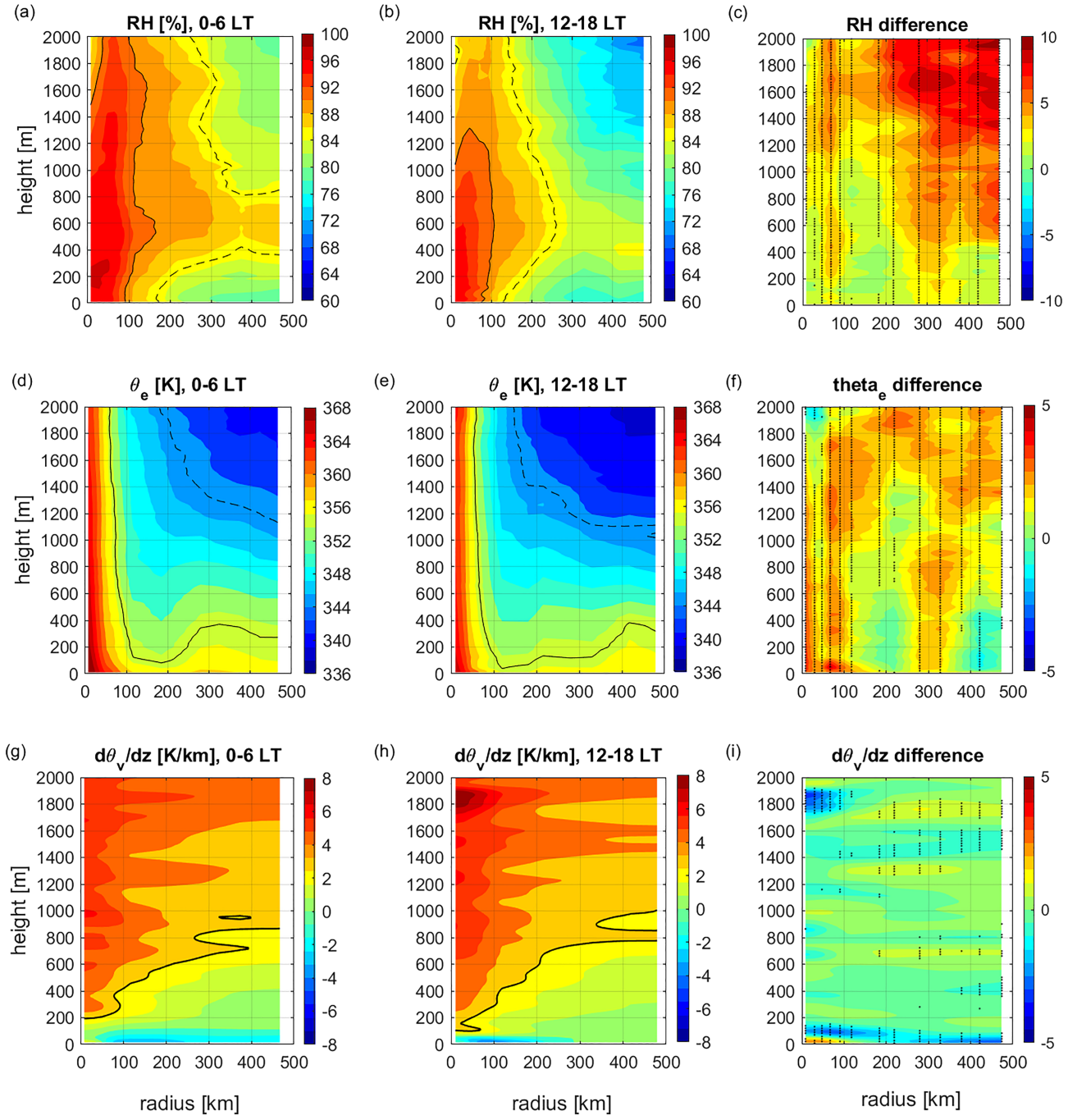

Figure 2. Dropsonde composites of relative humidity (a and b), equivalent potential temperature (θ_e, d and e), and vertical gradient of virtual potential temperature ($d\theta_v/dz$, g and h) for the night (0–6 LT, left panels) and afternoon (12–18 LT, middle panels) groups. In panels (a) and (b), the solid black line shows 90% contour, while the dashed line shows the 85% contour. In (d) and (e), the solid black line shows contour of 355 K, while the dashed line shows contour of 345 K. in (g) and (h), the black line shows the mixed layer depth denoted by contour of 3 K/km. The difference fields are shown in the right panels. The vertical stipples (black x) show regions where the difference is statistically significant at 95% confidence.

thermodynamic mixed layer depth denoted by the height of 3 K/km in the vertical gradient of virtual potential temperature (black line in Figures 2g and 2h), has similar values in the two composites. Note that the virtual potential temperature, θ_v, has the form of $\theta_v = \theta\ (1 + 0.61q)$. The mixed layer depth increases from ~200 m near the storm center to ~800 m at $R = 475$ km for both composites.

To further evaluate the diurnal cycle of the inflow structure in the TC boundary layer, we group the dropsonde data into four time windows: 0–6 LT, 6–12 LT, 12–18 LT, and 18–24 LT, similar to that presented in

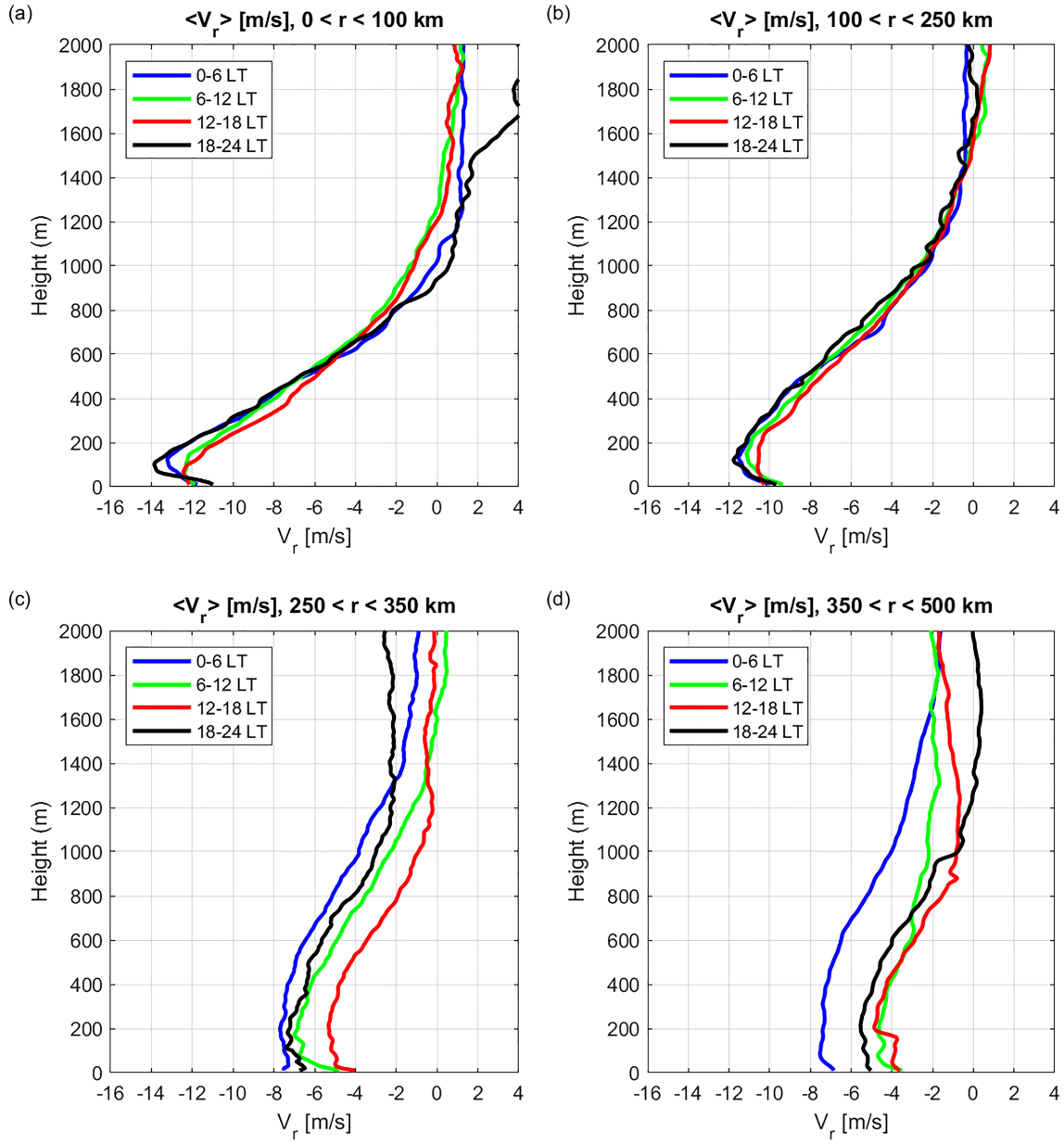

Figure 3. Plots of vertical profiles of the radial velocity averaged at different radial locations relative to the storm center for the four periods of interest: Night (0–6 LT), morning (6–12 LT), afternoon (12–18 LT), and evening (18–24 LT).

Dunion et al. (2014). We also split the data into radial bins as the composite analysis suggests that there are possible differences in the extents of the diurnal cycle signal at different radial locations (cf. Figures 1c and 1d). At R = 0–100 km (Figure 3a), the peak inflow is ~2 m/s stronger during the evening (18–24 LT) than during the morning (6–12 LT) or afternoon (12–18 LT). The outflow immediately above the inflow layer correlates with the boundary layer inflow in that the peak outflow is stronger for the nighttime groups (18–24 LT and 0–6 LT) than for the daytime (6–12 LT and 12–18 LT) groups. The inflow layer depth is also shallower in the nighttime groups than that in the daytime groups by ~100 m.

Interestingly, at R = 100–250 km (Figure 3b), the difference in the peak inflow between the nighttime and daytime groups is small, although the nighttime groups have slightly stronger inflow than the daytime groups. This region is typically referred to as the "moat region" where mesoscale subsidence occurs, which may prevent convective activity in this area of the storm, so that diurnal differences in the inflow strength

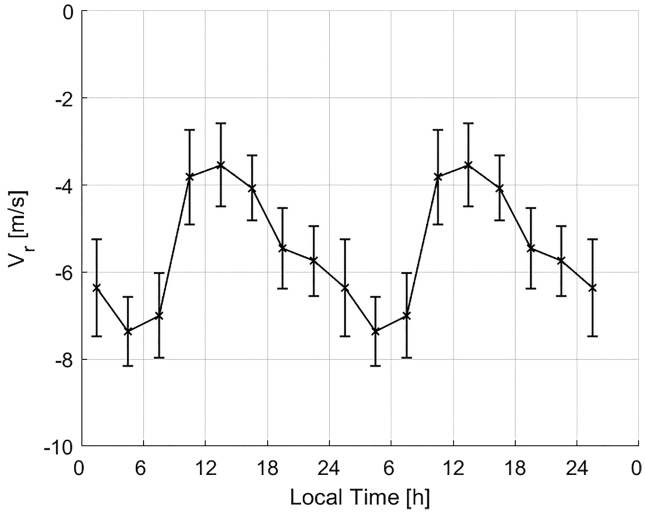

Figure 4. Plots of mean radial velocity averaged below 1,000 m altitude at 250–350 km radii as a function of local time. The error bars represent the 95% confidence interval.

are relatively small. Of note, Dunion et al. (2014, 2019) suggested that TC diurnal cycle is most active from 150–500 km radius, which is consistent with our result.

Figure 3 indicates that the diurnal cycle signal of the TC boundary layer inflow is equally strong in the 250–350 km and 350–500 km ranges where radially propagating diurnal pulses were clearly observed in the satellite data documented by Dunion et al. (2014). The peak inflow is largest in 0–6 LT group, while it is smallest in the 12–18 LT group (Figure 3c). The difference in the inflow strength between these two groups is as large as ~3 m/swhich is statistically significant based on two-tailed Student's *t* test. Below 2 km altitude, there is almost no outflow in all groups except the 6–12 LT group in which the outflow is very weak (<1 m/s). The inflow layer depth is larger in the nighttime groups than in the daytime groups.

At R = 350–500 km, only inflow is observed below 1.5 km altitude (Figure 3d). Again, the strength of the inflow is stronger at night than in day. Similar to the region of R = 250–350 km, the diurnal variation of the inflow strength is observed at this radius range (i.e., the boundary layer inflow increases from the afternoon to early evening and peaks after midnight then weakens again in the morning). Both the peak inflow and inflow layer depth are largest in the 0–6 LT group.

The mean inflow at R = 250–350 km, derived by averaging the data within the lowest 1,000 m in cylindrical coordinates, is shown in Figure 4 for different local time periods. Here, to better show the shape of the diurnal cycle, the data are grouped into eight periods. There is a clear diurnal signal for the boundary layer inflow, showing that inflow is strongest at night (0–6 LT) and weakest in the afternoon (12–18 LT). Interestingly, the diurnal oscillation is temporally asymmetric, with the strengthening inflow increasing slowly over a period of almost 18 hr, then quickly decreasing to its midday minimum amplitude in just 6 hr. Note that inflow is denoted as negative V_r here. One interpretation of this pattern is that the 250–350 km boundary layer inflow is disrupted during the passage of outward propagating squall lines which have their peak activity between 0 and 6 LT. The inflow recovers during the morning and appears to accelerate in the evening, perhaps as new squall lines are developing closer to the TC center. Future observational campaigns that use a combination of dropsondes and airborne or land-based radar observations may be able to support or refute this proposition.

4. Conclusions

This study analyzes over 2,000 GPS dropsondes collected in mature hurricane conditions to investigate the diurnal variation of the mean TC boundary layer structure. A composite analysis is conducted to compare the kinematic and thermodynamic structure of the boundary layer at night (0–6 LT) versus in the afternoon (12–18 LT). It is found that the boundary layer inflow is much stronger and deeper at night than in the afternoon. The boundary layer θ_e is also larger in the nighttime than in the daytime, especially for radii >150 km. The relative humidity is larger both in the inner core (R < 100 km) and outer-core regions in the night composite than in the afternoon composite. The near-surface boundary layer is more unstable in the outer-core region in the night composite than in the afternoon composite. Both the height of the maximum tangential wind speed and thermodynamic mixed layer depth are similar between the night and afternoon composites.

Grouping the dropsonde data into 6 hr windows relative to the local time shows a clear difference in the inflow strength between nighttime and daytime groups for all radii. The inflow is stronger during nighttime than during daytime. The amplitude of the diurnal cycle of the layer-averaged boundary layer inflow is largest at R = 250–350 km. Strong diurnal pulsing of convection in this region has also been observed in infrared satellite data by previous studies (e.g., Dunion et al., 2014). An important question remains regarding what drives the diurnal cycle of the radial inflow in the hurricane boundary layer. From a balanced dynamics perspective, the outflow at upper levels may be related to the boundary layer inflow. Numerical simulations show elevation of the outflow layer during the daytime (e.g., Dunion et al., 2019), which may

contribute to weaker outflow at upper levels during the daytime. Diurnal pulses have been suggested to exhibit squall line-like behaviors as they propagate away from the storm during the daytime (Dunion et al., 2019). Enhanced convection associated these features could act to enhance upper-level outflow at radii of 250–350 km during the day. It remains to be understood whether the enhanced convection during nighttime, perhaps supported by the moister boundary layer, causes the enhanced inflow, or whether enhanced inflow causes more convection.

Our findings of the diurnal cycle of TC boundary layer inflow and thermal structure are also consistent with signatures of a diurnal transverse circulation in both rotating and nonrotation frameworks as shown in several previous studies (Ciesielski et al., 2018; Navarro et al., 2017; Ruppert & Hohenegger, 2018; Ruppert & O'Neill, 2019). These studies illustrated an overnight intensification of bottom-heavy overturning driven by latent heating, and a daytime suppression of low-level overturning but with the outflow both strengthened and lifted in response to shortwave radiative heating. These circulation changes are largely balanced while the unbalanced component may be manifested as outward-propagating gravity waves (Evans & Nolan, 2019). It would be worthwhile to investigate the relationship between TC boundary layer structure changes in relationship to middle- and upper-level structure associated with the TC diurnal cycle in future studies.

Previous studies have also discussed the role of sea surface temperature (SST) in influencing diurnal variations of surface wind speed and boundary layer structure in cloud-free regions over the ocean (e.g., Betts et al., 1995; Brill & Albrecht, 1982; Kawai & Wada, 2007; Large & Caron, 2015). At outer radii, it is possible that SST varies diurnally, which needs to be evaluated in the future when collocated in situ SST observations are available. A newly developed dropsonde system that incorporates an infrared sensor to measure SST can help with this task (Zhang et al., 2017). Future study will also evaluate the effects of surface fluxes on boundary layer recovery in the context of the TC diurnal cycle.

Acknowledgments
This work was originally supported by NOAA's SHOUT project in which J. P. Dunion is the PI and J. A. Zhang is a co-I. D. S. Nolan and J. A. Zhang were supported by the NSF through Grant AGS1654831. J. A. Zhang also acknowledges supports from NSF Grant AGS1822128 and NOAA grant NA14NWS4680030. We acknowledge Altug Aksoy and Sim Aberson for their comments on an earlier version of the paper. We also want to thank Morgan O'Neill and James Ruppert for their constructive comments and suggestions that help substantially improve our paper. The dropsonde data are archived by NOAA's Hurricane Research Division (HRD) at this site (http://www.aoml.noaa.gov/hrd/data_sub/hurr.html). The final composite analysis result is archived at the ftp server of HRD and can be obtained at the following link: (ftp://ftp.aoml.noaa.gov/pub/hrd/jzhang/diurnal_sonde_composite).

References

Betts, A. K., Bretherton, C. S., & Klinker, E. (1995). Relation between mean boundary-layer structure and cloudiness at the R/V Valdivia during ASTEX. *Journal of the Atmospheric Sciences*, *52*, 2752–2762.

Betts, A. K., Fuentes, J. D., Garstang, M., & Bell, J. H. (2002). Surface diurnal cycle and boundary layer structure over Rondonia during the rainy season. *Journal of Geophysical Research*, *107*, 8065. https://doi.org/10.1029/2001JD000356

Bolton, D. (1980). The computation of equivalent potential temperature. *Monthly Weather Review*, *108*, 1046–1053. https://doi.org/10.1175/1520-0493(1980)108<1046:TCOEPT>2.0.CO;2

Bowman, K. P., & Fowler, M. D. (2015). The diurnal cycle of precipitation in tropical cyclones. *Journal of Climate*, *28*(13), 5325–5334.

Brill, K., & Albrecht, B. (1982). Diurnal variation of the trade-wind boundary layer. *Monthly Weather Review*, *110*(6), 601–613. https://doi.org/10.1175/1520-0493(1982)110<0601:DVOTTW>2.0.CO;2

Browner, S. P., Woodley, W. L., & Griffith, C. G. (1977). Diurnal oscillation of cloudiness associated with tropical storms. *Monthly Weather Review*, *105*, 856–864.

Ciesielski, P. E., Johnson, R. H., Schubert, W. H., & Ruppert, J. H. (2018). Diurnal cycle of the ITCZ in DYNAMO. *Journal of Climate*, *31*, 4543–4562. https://doi.org/10.1175/JCLI-D-17-0670.1

Ditchek, S. D., Corbosiero, K. L., Fovell, R. G., & Molinari, J. (2019). Electrically active tropical cyclone diurnal pulses in the Atlantic basin. *Monthly Weather Review*, *147*(10), 3595–3607. https://doi.org/10.1175/MWR-D-19-0129.1

Ditchek, S. D., Molinari, J., Corbosiero, K. L., & Fovell, R. G. (2019). An objective climatology of tropical cyclone diurnal pulses in the Atlantic basin. *Monthly Weather Review*, *147*, 591–605. https://doi.org/10.1175/MWR-D-18-0368.1

Dunion, J. P., Thorncroft, C. D., & Nolan, D. S. (2019). Tropical cyclone diurnal cycle signals in a hurricane nature run. *Monthly Weather Review*, *147*(1), 363–388. https://doi.org/10.1175/MWR-D-18-0130.1

Dunion, J. P., Thorncroft, C. D., & Velden, C. S. (2014). The tropical cyclone diurnal cycle of mature hurricanes. *Monthly Weather Review*, *142*, 3900–3919.

Evans, R. C., & Nolan, D. S. (2019). Balanced and radiating wave responses to diurnal heating in tropical cyclone-like vortices using a linear nonhydrostatic model. *Journal of the Atmospheric Sciences*, *76*, 2575–2597. https://doi.org/10.1175/JAS-D-18-0361.1

Gray, W. M., & Jacobson, R. W. (1977). Diurnal variation of deep cumulus convection. *Monthly Weather Review*, *105*, 1171–1188.

Holtslag, A. A., Svensson, G., Baas, P., Basu, S., Beare, B., Beljaars, A. C. M., et al. (2013). Stable atmospheric boundary layers and diurnal cycles. *Bulletin of the American Meteorological Society*, *94*, 1692–1706.

Kawai, Y., & Wada, A. (2007). Diurnal Sea surface temperature variation and its impact on the atmosphere and ocean: A review. *Journal of Oceanography*, *63*, 721–744.

Knaff, J. A., Slocum, C. J., & Musgrave, K. D. (2019). Quantification and exploration of diurnal oscillations in tropical cyclones. *Monthly Weather Review*, *147*, 2105–2121.

Kossin, J. P. (2002). Daily hurricane variability inferred from GOES infrared imagery. *Monthly Weather Review*, *130*(9), 2260–2270.

Kumar, V., Svensson, G., Holtslag, A. A. M., Parlange, M. B., & Meneveau, C. (2010). Impact of surface flux formulations and geostrophic forcing on large-eddy simulations of the diurnal atmospheric boundary layer flow. *Journal of Applied Meteorology and Climatology*, *49*, 1496–1516.

Large, W. G., & Caron, J. M. (2015). Diurnal cycling of sea surfacetemperature, salinity, and current inthe CESM coupled climate model. *Journal of Geophysical Research: Oceans*, *120*, 3711–3729. https://doi.org/10.1002/2014JC010691

Leppert, K. D., & Cecil, D. J. (2016). Tropical cyclone diurnal cycle as observed by TRMM. *Monthly Weather Review*, *144*(8), 2793–2808.

Liu, C., & Moncrieff, M. W. (1998). A numerical study of the diurnal cycle of tropical oceanic convection. *Journal of the Atmospheric Sciences*, *55*(13), 2329–2344. https://doi.org/10.1175/1520-0469(1998)055<2329:ANSOTD>2.0.CO;2

Liu, S., & Liang, X. (2010). Observed diurnal cycle climatology of planetary boundary layer height. *Journal of Climate*, *23*, 5790–5809.

Melhauser, C., & Zhang, F. (2014). Diurnal radiation cycle impact on the pregenesis environment of hurricane Karl (2010). *Journal of the Atmospheric Sciences*, *71*(4), 1241–1259.

Mellor, G. L., & Yamada, T. (1974). A hierarchy of turbulence closure models for planetary boundary layers. *Journal of the Atmospheric Sciences*, *31*(7), 1791–1806. https://doi.org/10.1175/1520-0469(1974)031<1791:AHOTCM>2.0.CO;2

Navarro, E. L., Hakim, G. J., & Willoughby, H. E. (2017). Balanced response of an axisymmetric tropical cyclone to periodic diurnal heating. *Journal of the Atmospheric Sciences*, *74*(10), 3325–3337. https://doi.org/10.1175/JAS-D-16-0279.1

Nolan, D. S., Atlas, R., Bhatia, K. T., & Bucci, L. R. (2013). Development and validation of a hurricane nature run using the joint OSSE nature run and the WRF model. *Journal of Advances in Modeling Earth Systems*, *5*, 382–405. https://doi.org/10.1002/jame.20031

O'Neill, M. E., Perez-Betancourt, D., & Wing, A. A. (2017). Accessible environments for diurnal-period waves in simulated tropical cyclones. *Journal of the Atmospheric Sciences*, *74*(8), 2489–2502. https://doi.org/10.1175/JAS-D-16-0294.1

Randall, D. A., Harshvardhan, R., & Dazlich, D. A. (1991). Diurnal variability of the hydrologic cycle in a general circulation model. *Journal of the Atmospheric Sciences*, *48*(1), 40–62. https://doi.org/10.1175/1520-0469(1991)048<0040:DVOTHC>2.0.CO;2

Ruppert, J. H., & Hohenegger, C. (2018). Diurnal circulation adjustment and organized deep convection. *Journal of Climate*, *31*(12), 4899–4916. https://doi.org/10.1175/JCLID-17-0693.1

Ruppert, J. H., & O'Neill, M. E. (2019). Diurnal cloud and circulation changes in simulated tropical cyclones. *Geophysical Research Letters*, *46*, 502–511. https://doi.org/10.1029/2018GL081302

Svensson, G. and Coauthors (2011). Evaluation of the diurnal cycle in the atmospheric boundary layer over land as represented by a variety of single column models—The second GABLS experiment. *Boundary-Layer Meteorology, 140*, 177–206, 2, DOI: https://doi.org/10.1007/s10546-011-9611-7

Tang, X., & Zhang, F. (2016). Impacts of the diurnal radiation cycle on the formation, intensity, and structure of hurricane Edouard (2014). *Journal of the Atmospheric Sciences*, *73*(7), 2871–2892. https://doi.org/10.1175/JAS-D-15-0283.1

Wu, Q., & Ruan, Z. (2016). Diurnal variations of the areas and temperatures in tropical cyclone clouds. *Quarterly Journal of the Royal Meteorological Society*, *142*(700), 2788–2796. https://doi.org/10.1002/qj.2868

Yang, G.-Y., & Slingo, J. (2001). The diurnal cycle in the tropics. *Monthly Weather Review*, *129*(4), 784–801. https://doi.org/10.1175/1520-0493(2001)129<0784:TDCITT>2.0.CO;2

Zhang, J. A., Cione, J. J., Kalina, E. A., Uhlhorn, E. W., Hock, T., & Smith, J. A. (2017). Observations of infrared sea surface temperature and air-sea interaction in hurricane Edouard (2014) using GPS dropsondes. *Journal of Atmospheric and Oceanic Technology*, *34*(6), 1333–1349. https://doi.org/10.1175/JTECH-D-16-0211.1

Zhang, J. A., Rogers, R. F., Nolan, D. S., & Marks, F. D. Jr. (2011). On the characteristic height scales of the hurricane boundary layer. *Monthly Weather Review*, *139*(8), 2523–2535. https://doi.org/10.1175/MWR-D-10-05017.1

Zhang, J. A., Rogers, R. F., Reasor, D. P., Uhlhorn, E. W., & Marks, F. D. Jr. (2013). Asymmetric hurricane boundary layer structure from dropsonde composites in relation to the environmental vertical wind shear. *Monthly Weather Review*, *141*(11), 3968–3984. https://doi.org/10.1175/MWR-D-12-00335.1

References From the Supporting Information

Landsea, C. W., & Franklin, J. L. (2013). Atlantic hurricane database uncertainty and presentation of a new database format. *Monthly Weather Review*, *141*, 3576–3592. https://doi.org/10.1175/MWR-D-12-00254.1

Willoughby, H. E., & Chelmow, M. B. (1982). Objective determination of hurricane tracks from aircraft observations. *Monthly Weather Review*, *110*(9), 1298–1305. https://doi.org/10.1175/1520-0493(1982)110<1298:ODOHTF>2.0.CO;2